tvst

Article

Three-Dimensional Distribution Of Fundus Depolarization and Associating Factors Measured Using Polarization-Sensitive Optical Coherence Tomography

Asahi Fujita[1,2], Tatsuaki Amari[1,3], Kohei Ueda[1], Keiko Azuma[1], Tatsuya Inoue[1,4], Kayoko Komatsu[1], Motoshi Yamamoto[1], Nobuyori Aoki[5], Masahiro Yamanari[5], Satoshi Sugiyama[5], Makoto Aihara[1], Satoshi Kato[1], and Ryo Obata[1]

[1] Department of Ophthalmology, The University of Tokyo Hospital, Tokyo, Japan
[2] Tokyo Metropolitan Geriatric Hospital, Tokyo, Japan
[3] Eguchi Eye Hospital, Hakodate, Japan
[4] Department of Ophthalmology, Yokohama City University Medical Center, Yokohama, Japan
[5] Tomey Corporation, Nagoya, Japan

Correspondence: Ryo Obata, Department of Ophthalmology, Graduate School of Medicine, University of Tokyo, 7-3-1 Hongo, Bunkyo-ku, Tokyo 113-8655, Japan. e-mail: robata-tky@umin.ac.jp

Received: May 28, 2020
Accepted: January 3, 2021
Published: February 18, 2021

Keywords: polarization-sensitive optical coherence tomography; melanin pigmentation; distribution

Citation: Fujita A, Amari T, Ueda K, Azuma K, Inoue T, Komatsu K, Yamamoto M, Aoki N, Yamanari M, Sugiyama S, Aihara M, Kato S, Obata R. Three-dimensional distribution of fundus depolarization and associating factors measured using polarization-sensitive optical coherence tomography. Trans Vis Sci Tech. 2021;10(2):30, https://doi.org/10.1167/tvst.10.2.30

Purpose: To investigate the three-dimensional distribution and associating demographic factors of depolarization, using polarization-sensitive optical coherence tomography (PS-OCT), to evaluate melanin pigmentation in the retinal pigment epithelium (RPE) and choroid in healthy eyes.

Methods: In total, 39 unaffected healthy eyes of 39 subjects were examined using a PS-OCT clinical prototype. The degree of depolarization, expressed as the polarimetric entropy, was assessed in the RPE, the superficial and the total choroid layer, especially in the center, the inner, or the outer areas centered at the fovea. The values and their association with the demographic data were analyzed. Near-infrared fundus autofluorescence (NIRAF) was also used, in the same manner, for the comparison. Twenty-eight of 39 eyes were measured twice to evaluate intrasession repeatability.

Results: Both the polarimetric entropy in the RPE and the gray level in NIRAF, decreased from the center to the periphery ($P < 0.001$). The polarimetric entropy in the RPE was significantly associated with age in each area ($P \leq 0.001$). In the RPE and the superficial choroid, the polarimetric entropy was negatively associated with axial length in each area ($P \leq 0.002$). The intraclass correlation coefficient of the polarimetric entropy in the same session was excellent in each area of the RPE, superficial choroid, or total choroid layer (0.94–0.98).

Conclusions: The distribution of fundus melanin pigment-related depolarization was evaluated using PS-OCT. The depolarization was associated with the subjects' demographic data, such as age or axial length.

Translational Relevance: The presented information in healthy eyes provides an essential basis for the investigation into a variety of chorioretinal pathologies.

Introduction

Melanin is a basic pigment that is essential to normal eye function.[1,2] Melanin pigmentation is observed in the retinal pigment epithelium (RPE) and choroid.[3] Spatial distribution or association with demography, such as age or race, has been reported in the normal human donor eye.[4] Melanin pigmentation acts as an absorber of scattered light, reduces oxidative stress, protects RPE from lipofuscin damage, and stores the essential nutrient zinc.[5–8] Hence, it has attracted great interest in understanding the pathological process of ocular diseases, such as age-related macular degeneration[9] or Vogt-Koyanagi-Harada disease.[10,11]

A number of researchers have used imaging modalities for qualitative and quantitative evaluations of melanin pigmentation in the RPE and the choroid. In vitro and ex vivo use of high-magnification micrographs or pathological specimens have been reported.[12–15] However, postmortem human eyes from donors or animal eyes were used in those methods, making it difficult to apply these approaches to the eyes of living individuals.

Near-infrared fundus autofluorescence (NIRAF) is speculated to mainly originate from melanin,[16–19] but it is also suspected that the signal in NIRAF is affected by lipofuscin and reflected light.[16,20] NIRAF imaging is useful in clinical settings because it is noninvasive and repeatable and can be detected through confocal scanning laser ophthalmoscopy, which is commercially available.[5] However, autofluorescence (AF) cannot resolve the signal from the RPE, the sensory retina, or the choroid clearly.[16] Also, the AF intensity was displayed as a relative value, making quantitative assessment difficult. Recently the imaging of RPE cells using adaptive optics technique has been reported, but the cone fluorescence was also reflected on the image, and the measurement area was relatively limited in the current settings.[21,22] Directional optical coherence tomography (OCT) measured differences in directional scattering from the retina in mice.[23] The RPE showed high reflectivity but low directionality compared with other melanin-free layers, suggesting the potential of quantifying the melanin pigmentation.[23]

Detecting multiply scattered light, that is, depolarization is also an alternative to assess melanin. Depolarization can be caused by the RPE, but melanocytes, melanin-containing inflammatory cells, and hard exudates were also depolarizing structures.[24] Previous reports studied the light scattering of the RPE by measuring depolarization with scanning laser polarimetry (SLP)[25–28] or polarization-sensitive optical coherence tomography (PS-OCT).[27,29–40] With SLP, multiply scattered light was emphasized by detecting depolarized light and rejecting light that retains polarization,[25,27] and the potential to evaluate macular diseases was demonstrated.[26–28] On the distribution of polarization signal evaluated by SLP, phase retardation profiles that could reflect mainly Henle fiber layer changed with age.[41] Additionally, the average of macular depolarization increased with age in the normal eye.[42] SLP might be able to detect small drusen and subtle leakage by using the scattered light images that have the potential to be more sensitive than confocal images.[43] However, SLP provides a weighted average of several retinal layers and the RPE, and is not depth-resolved.[43]

PS-OCT can detect tissues' depth-resolved polarization properties and provide additional tissue-specific contrast in cross-sectional or three-dimensional images.[29,40,44] PS-OCT detects melanin-containing structures, such as the RPE and the choroid, as polarization-scrambling layers.[27,31,32] PS-OCT can segment different retinal layers, based on their intrinsic polarization properties, and identify or analyze changes in eyes with pathological conditions. Therefore it enables three-dimensional assessment of melanin pigmentation in the RPE or the choroid in eyes with retinal or macular diseases, as previously reported.[27,33–35] Quantitative analysis between the degree of polarization and melanin pigmentation in the RPE or the choroid was also investigated in vitro, using rodent models or in small series of healthy volunteers.[36–39] However, the connections between the distribution of depolarization in the RPE or the choroid and basic demographic and biometric parameters have not been evaluated in clinical settings.

From technical perspectives, almost all the previous studies of PS-OCT used the degree of polarization uniformity (DOPU) to parameterize the depolarization of light. Although it has been shown that the DOPU is useful to visualize and quantify the depolarization in the fundus, a recent study pointed out that the DOPU depended on the incident state of polarization.[45] Because the incident state of polarization at the RPE and the choroid can be changed by birefringence of overlaying tissues, for example, cornea, retinal nerve fiber, and scar tissue, it is desired and has been suggested to use depolarization metrics that are insensitive to the incident state of polarization.[30,45,46] Another important feature that depolarization metrics should have is correcting noise bias,[30,47] because both the depolarizing property of tissues and random noise increase the randomness of measured state of polarization. Among the depolarization metrics to date, only the polarimetric entropy has both features of the insensitivity to the incident state of polarization and the noise-bias correction.[30] In addition, we recently showed that the polarimetric entropy was linearly proportional to melanin concentration in a double logarithmic scale.[48]

This study aimed to investigate the three-dimensional distribution of tissue depolarization as a biomarker of melanin pigmentation in the RPE and the choroid. We measured the healthy fellow eye of patients using a clinical prototype of PS-OCT and analyzed the reproducibility of the polarimetric entropy. We then analyzed the statistical correlation between the polarimetric entropy and the physical factors of the subjects.

Methods

Subjects' Inclusion and Exclusion

The Research Ethics Committee of the Graduate School of Medicine and Faculty of Medicine at The University of Tokyo (Tokyo, Japan) approved this single-center, cross-sectional study. It was performed according to the tenets of the Declaration of Helsinki. Each subject provided written informed consent after the nature and possible consequences of this study were explained.

We included 39 eyes of 39 Asian (dark brown iris color) subjects who visited the Macular Clinic at the University of Tokyo Hospital between March 2018 and September 2019 for unilaterally affected macular diseases. The unaffected eye was used for this study. All subjects underwent comprehensive ophthalmic examination, including refractive error evaluation, best-corrected visual acuity, intraocular pressure, anterior segment examination, and fundus biomicroscopy with pupil dilation. In addition, spectral domain OCT (Spectralis OCT; Heidelberg Engineering, Heidelberg, Germany), infrared reflectance, and NIRAF imaging with scanning laser ophthalmoscopy (HRA2, Retinal Angiograph 2; Heidelberg Engineering) were performed. After the examination, eyes with abnormal findings associated with retinal or macular diseases were excluded from this study. The axial length was measured with an optical biometer (OA-2000; Tomey Corp., Nagoya, Japan).

PS-OCT Imaging

PS-OCT measurement was performed using a clinical prototype for retinal imaging (Tomey Corp.). The principle of our PS-OCT was demonstrated for imaging of the anterior eye segment previously.[49] PS-OCT for retinal imaging was also demonstrated using the same principle,[48,50] which was used in this study. See Supplementary Figure S1 for a schematic diagram of the interferometric system. In brief, the system was based on swept-source OCT technology. The light source was a wavelength-swept laser (Axsun Technologies, Billerica, MA, USA) with a repetition rate of 100 kHz and a center wavelength of 1050 nm. Unlike conventional swept-source that mathematically characterizes the target's polarization property, it consists of fiberoptic components (Optizone Technology Limited, Shenzhen, China) and four balanced photodetectors (PDB481C-AC; Thorlabs, Inc., Newton, NJ, USA) that receive interferometric signals of the Jones matrix in a parallel manner. An area of 20° (approximately 6 mm) by 20° (approximately 6 mm) was scanned with 512 A-lines (horizontal) × 512 B-scans (vertical) in 3.3 seconds. The pixel size of each B-scan was 6/512B-scan = 11.7 μm. The size of each pixel in the B-scan was H: 6/512A = 11.7μm, and V: 4.3 μm. Polarization-independent intensity images were obtained by averaging Jones matrix element intensities. The polarization scrambling or depolarization of the sample was parameterized as polarimetric entropy, which showed spatial randomness of the polarization property through statistical characterization of the measured Jones matrix.[30] Kernel size for polarimetric entropy calculation was 11 × 7 pixels, which corresponds to 128.7 × 30.1 μm. Specifically, the measured Jones matrix was converted to a 4 × 4 covariance matrix to treat the statistical property of the Jones matrix. Note that the covariance matrix held the same information as the Mueller matrix but was highly linked to eigenanalysis mathematically. The polarimetric entropy was defined in a von Neumann sense and derived from eigenvalues of the spatially ensemble-averaged covariance matrix. The details of the derivation were described previously.[19,30] In 28 of 39 eyes, the PS-OCT images were obtained twice to assess intrasession repeatability.

Subsequently, the polarimetric entropy of the RPE and the choroid was analyzed in three image layers, as described below. The axial scan range was 4.44 mm in the eye. The axial resolution in tissue was 8.6 μm (4.3 μm × 2.0 pixels). Specifically, after obtaining the three-dimensional PS-OCT dataset, automatic segmentation was performed at the RPE-Bruch's membrane (BM) complex and chorioscleral interface (CSI) in the intensity B-scan images, using a built-in automatic segmentation algorithm, which delineates the segmentation curve on the basis of the signal intensity. Subsequently, the RPE layer was defined as five pixels (22 μm) anterior and posterior to the RPE-BM complex. The "Superficial Choroid" layer was defined as 10–20 pixels (44–88 μm) posterior to the RPE-BM complex. The "Total Choroid" layer was defined as between 10 pixels (44 μm) posterior to the RPE-BM complex and CSI. Within each of the three layers, the average polarimetric entropy value along each A-line was calculated and plotted in two-dimensional en face fundus maps. In addition, choroidal thickness was defined by the distance between the RPE-BM complex and CSI.

Image Analysis

Using the built-in software, the Early Treatment Diabetic Retinopathy Study grid was overlaid on the en face polarimetric entropy or choroidal thickness map. The diameters of the center, inner, and outer circles

were 1, 3, and 6 mm, respectively, centered on the fovea. The projected grid size was corrected according to the axial length in each eye using a modified Benette's formula so that the grid on the retina had the same diameter (mm) irrespective of different axial lengths.[51] The location was identified by referring to the cross-sectional B-scan intensity images. The "center" area, representing the area within the center circle, the "inner ring" area between the center and the inner circles, and the "outer ring" area between the inner and the outer circles were defined (See Supplementary Fig. S2). The mean values of the polarimetric entropy or choroidal thickness in each area of the three layers were calculated.

NIRAF Imaging

NIRAF images were obtained using a light source at 786 nm with a barrier filter at 830 nm to separate excitation from fluorescence. The images were acquired at 30° × 30° and centered on the fixation point with 768 × 768 pixels. Using the built-in eye-tracking system, 100 consecutive images were averaged. The image was exported to the ImageJ software (U.S. National Institute of Health, Bethesda, MD, USA),[52] which is publicly accessible. Similar to PS-OCT data, the Early Treatment Diabetic Retinopathy Study grid, corrected by the axial length, was overlaid. The average gray level, which represented NIRAF at each pixel, was computed. Because the gray level should be interpreted as a relative value within the same image, two relative values were calculated for the analyses. The "inner ring/center" value was defined as the mean value in the inner ring area divided by the mean value recorded in the center area, and the "outer ring/center" value was defined as the mean value in the outer ring area divided by the mean value measured in the center area.

Statistical Analysis

The intraclass correlation coefficient of the polarimetric entropy or choroidal thickness in each area of the three layers in 28 eyes was evaluated to assess the intrasession repeatability. The value was determined based on previously reported criteria.[53]

Relative values of polarimetric entropy to the center area were calculated to compare the results of the PS-OCT data with those of NIRAF. Distribution of the absolute or relative polarimetric entropy in the center, inner, or outer rings at the RPE, superficial choroid, or total choroid layers was assessed using the Wilcoxon signed-rank test. Associations between the absolute or relative polarimetric entropy value from PS-OCT, the relative gray level from NIRAF at each area of each layer, and age or axial length were analyzed using Spearman's rank correlation coefficient. Associations between these values and sex were analyzed using Wilcoxon signed-rank test. Additionally, in the present study, approximately half the subjects had pachychoroid spectrum disease (PSD)[54] in the unstudied fellow eyes. PSD includes central serous chorioretinopathy (CSC), pachychoroid pigment epitheliopathy, pachychoroid neovasculopathy, or focal choroidal excavation (FCE), which share some anatomic features, such as diffuse or focal thickening of the choroid, choroidal vascular hyperpermeability, or RPE abnormalities. Previous studies reported that subjects affected with unilateral PSD could show some characteristic choroidal findings in the contralateral healthy eyes.[55,56] We also analyzed the association between the polarimetric entropy and having PSD in the fellow eye using the Wilcoxon signed-rank test to investigate the difference in choroidal melanin pigmentation between eyes with PSD in the fellow eye and those without. If multiple factors were significantly associated with an objective variable in these univariate analyses, then multiple linear regression test was added.

All statistical analyses were performed using the statistical programming language 'R' (R version 3.4.3; The Foundation for Statistical Computing, Vienna, Austria). The threshold for significance was $P < 0.05$.

Table 1. Demographic Data

Age, years, mean ± SD [range]	52.6 ± 14.5 [24–78]
Sex, male, n, %	27/39, 69.2%
Laterality, n (%)	
Right	17 eyes (43.6%)
Left	22 eyes (56.4%)
Axial Length, mm (mean ± SD) [range]	24.6 ± 1.64 [22.1–29.9]
Presence of PSD in the fellow eye, n (%)	18 eyes (46.2%)

SD, standard deviation.

Results

We examined 39 normal eyes of 39 subjects. The average age was 52.6 ± 14.5 years (range, 24–78 years). The axial length was 24.6 ± 1.64 mm (22.1–29.9 mm). The demographic data are shown in Table 1. The fellow eye had CSC (15 cases), retinal vein occlusion (five cases), age-related macular degeneration (three cases),

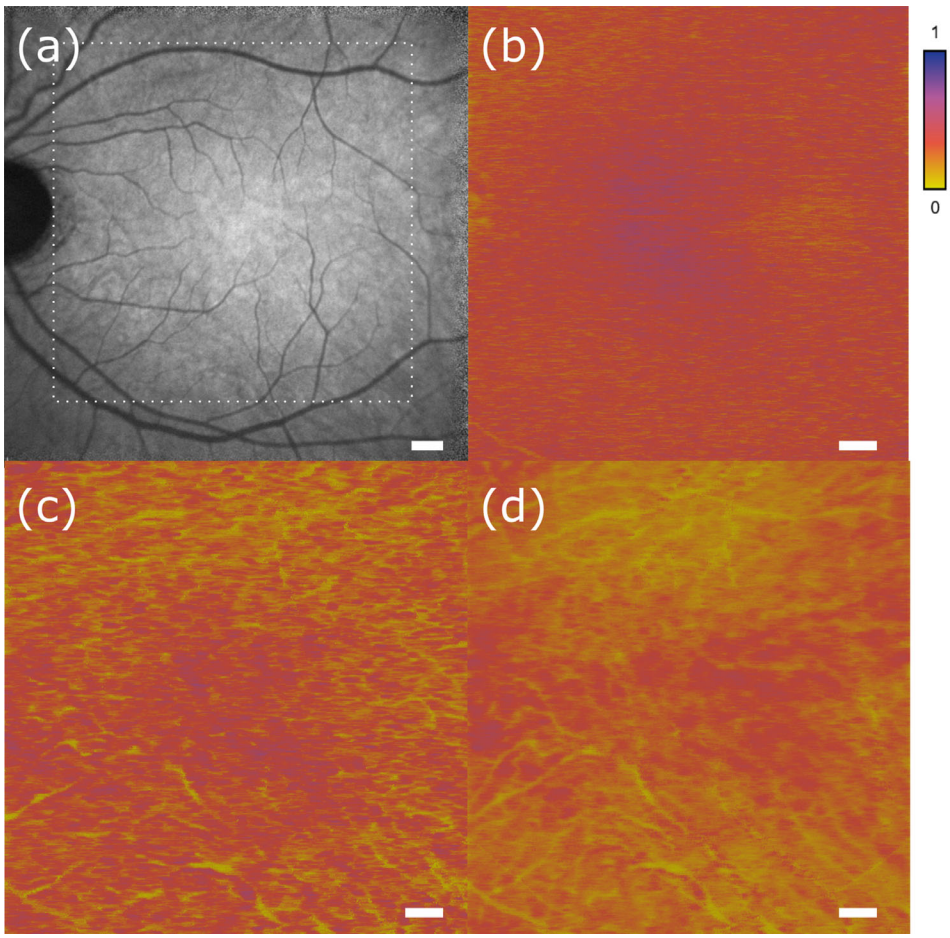

Figure 1. Representative images of the NIRAF and the intensity/entropy from PS-OCT in the healthy eye of a 53-year-old female. (a) NIRAF image. The dotted square indicates the location corresponding to the entropy maps (b, c, and d). (b) Entropy map of the RPE (median [range] 0.27 [0.095–0.51], mean ± SD; COV 0.28 ± 0.044; 0.16). (c) Entropy map of the superficial choroid (median [range] 0.26 [0.084–0.47], mean ± SD; COV 0.26 ± 0.048; 0.18). (d) Entropy map of the total choroid (median [range] 0.22 [0.000–0.52], mean ± SD; COV 0.23 ± 0.064; 0.28). The pseudo-color map of the entropy covered full range from 0 to 1 in which the entropy was defined. *Scale bar:* 500 µm. The *color scale* in the upper right represents entropy [AU].

FCE (three cases), vitreoretinal interface disease (three cases), myopic-related disease (two cases), retinal artery occlusion (two cases), choroidal tumor (two cases), idiopathic choroidal neovascularization (one case), pit macular syndrome (one case), macular microhole (one case), and Coats disease (one case). Eighteen fellow eyes (46.2%) were affected by CSC or FCE, which were considered PSD.

Representative images of the NIRAF and polarimetric entropy obtained from PS-OCT are shown in Figure 1. The distribution of the mean polarimetric entropy in each area of each layer is shown in Figure 2. The polarimetric entropy in the RPE and the gray level in NIRAF were significantly decreased from the center to the periphery. On the other hand, polarimetric entropy in the superficial choroid was comparable between all areas. The polarimetric entropy in the total choroid was higher in the outer ring than the center or inner rings (Fig. 2). The relative value of polarimetric entropy in the RPE at the inner or outer rings to the center in PS-OCT, and the relative gray level of the inner and outer rings in NIRAF significantly decreased from the inner to the outer ring. (See Supplementary Fig. S3). The intraclass correlation coefficients of polarimetric entropy and choroidal thickness, shown in Table 2, fell into the "excellent" category,[53,57] indicating high reproducibility of the values obtained with PS-OCT.

We also investigated the association between the polarimetric entropy of PS-OCT in each layer, the relative gray level of NIRAF, and the subjects' background characteristics (e.g., age, axial length, sex, and choroidal thickness). The polarimetric entropy at the RPE layer in each area was significantly positively

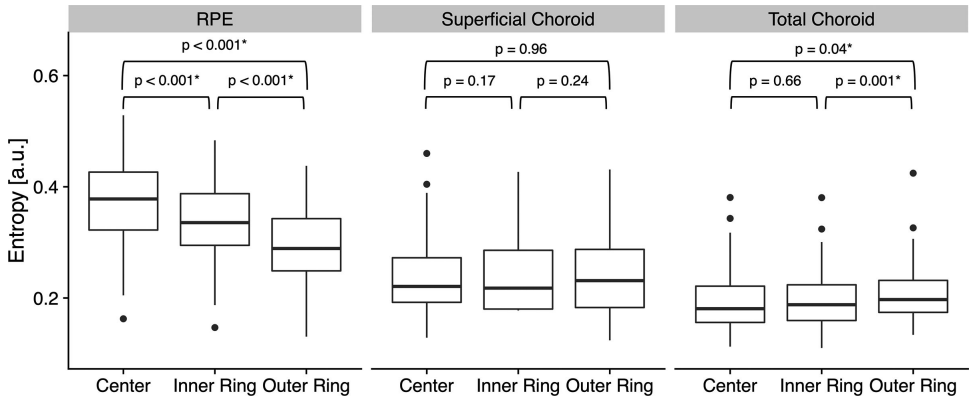

Figure 2. Box plots showing the entropy at the center, inner ring, and outer ring in each layer measured with PS-OCT. The *central bold line* indicates the median. The lower and upper ends of the box indicate the lower and upper quartile, respectively. Interquartile range (IQR) is defined as the difference between upper and lower quartiles. The *upper whisker* represents "upper quartile + 1.5 × IQR", and the *lower whisker* represents "lower quartile-1.5 × IQR." *Black dots* indicate outliers. Distribution of the polarimetric entropy in the center, inner, or outer rings was assessed using the Wilcoxon signed-rank test at the RPE, superficial choroid or total choroid layers, respectively. a.u., Arbitrary unit.

Table 2. ICC Values of Entropy in Each Area of the RPE, Superficial Choroid, or Total Choroid and the Choroidal Thickness

	Center	Inner Ring	Outer Ring
Entropy			
RPE	0.953 [0.901–0.978]	0.957 [0.910–0.980]	0.976 [0.950–0.989]
Superficial choroid	0.943 [0.882–0.973]	0.953 [0.902–0.978]	0.966 [0.928–0.984]
Total choroid	0.979 [0.955–0.990]	0.982 [0.962–0.992]	0.982 [0.962–0.992]
Choroidal thickness	0.980 [0.958–0.991]	0.985 [0.968–0.993]	0.992 [0.982–0.996]

ICC values are shown with 95% confidence interval in [ ].
ICC, intraclass correlation coefficient.

associated with age ($P < 0.01$, respectively). The scatter plots of the polarimetric entropy in the RPE or the superficial choroid layer versus age are shown in Figure 3. The polarimetric entropy increased with age in the RPE in each section, but not in the superficial choroid layer. Representative PS-OCT images of a young subject (age, 24 years old; AL, 25.5 mm) and an aged patient (age, 74 years old; AL, 24.7 mm) are shown in Figure 4. Both subjects showed normal configuration in B-scan images crossing the fovea. In the B-scan, the polarimetric entropy at the RPE layer looked higher in the aged subject, which was confirmed by the en face polarimetric entropy maps at the RPE segment. The en face polarimetric entropy map at the superficial choroid or the total choroid did not show such a remarkable difference (Fig. 4). The relative ratio of the polarimetric entropy in the inner ring to the center did not change with age, while that of the outer ring to the center increased with age both in the polarimetric entropy at the RPE and the gray level in NIRAF ($P = 0.04$, $P < 0.01$, respectively; see Supplementary Fig. S4).

The scatter plots of the polarimetric entropy in the RPE or the superficial choroid layer versus axial length are shown in Figure 5. In the RPE and the superficial choroid layers, polarimetric entropy was negatively correlated with axial length in each area ($P < 0.01$, respectively; Fig. 5). In each section, a significant association of the polarimetric entropy in the RPE with age and axial length was recognized by multiple regression test. In the multiple regression test, both age and axial length were associated with the polarimetric entropy in the RPE in each area. The polarimetric entropy in PS-OCT and the relative gray level in NIRAF did not have a significant correlation with sex. Having PSD in the fellow eye was not significantly associated with the mean polarimetric entropy in the RPE, the superficial choroid, or the total choroid from PS-OCT or the relative intensity in NIRAF (See Supplementary Table S1). The polarimetric entropy in

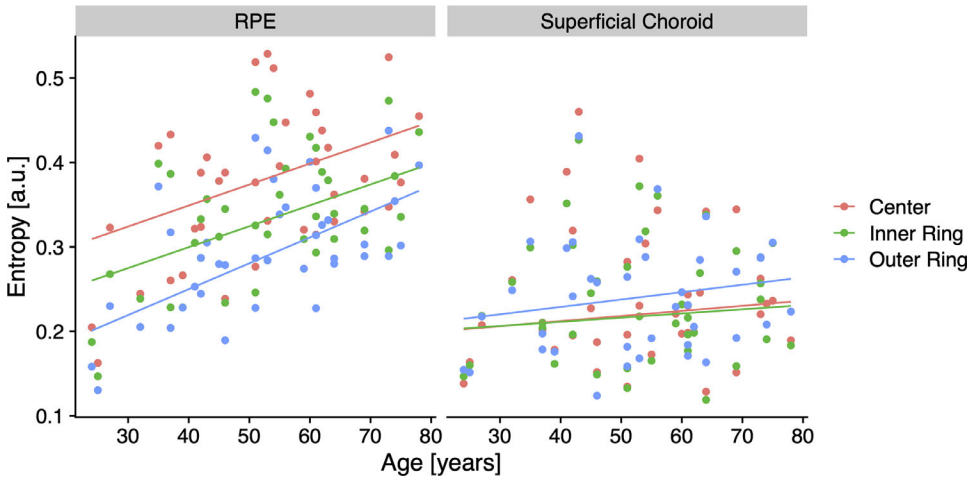

Figure 3. Scatter plots showing the relationship between age and the entropy in the center (*red*), the inner ring (*green*), or the outer ring (*blue*) at the RPE (*left*) and the superficial choroid layer (*right*). *Red line*, *green line*, or *blue line* were the regression lines from the data in the center, the inner ring, or the outer ring, respectively. Age showed fair correlation with the entropy in the RPE in all areas, center, inner ring, outer ring ($r = 0.42$ [$P = 0.008$], $r = 0.46$ [$P = 0.003$], $r = 0.52$ [$P < 0.001$], respectively; Spearman's rank correlation coefficient). On the other hand, age did not show significant correlation with the entropy in the superficial choroid layer in any area ($r = 0.07$ [$P = 0.69$], $r = 0.02$ [$P = 0.90$], $r = 0.17$ [$P = 0.29$], respectively [N = 39]; Spearman's rank correlation coefficient).

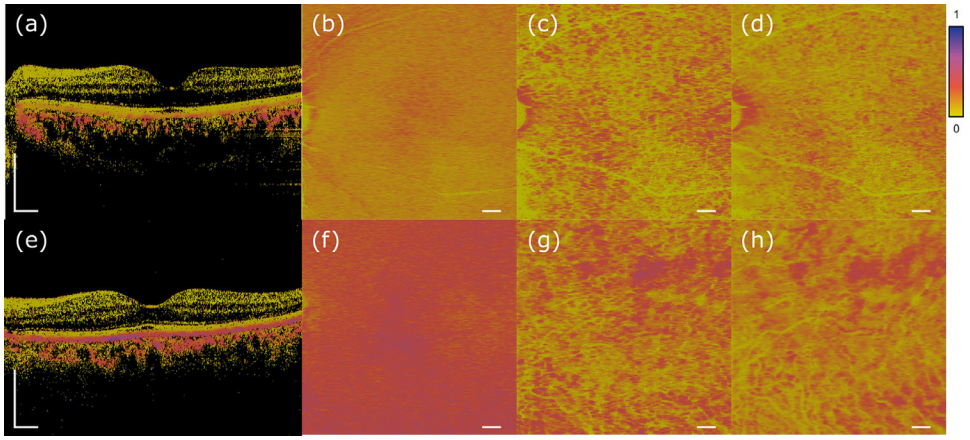

Figure 4. Representative PS-OCT images of a young subject (a, b, c, and d: age, 24 years old; AL, 25.5 mm) and those of an aged subject (e, f, g, and h: age, 74 years old; AL, 24.7 mm). Both subjects showed normal configuration in B-scan images crossing the fovea (a and e). In the B-scan, the entropy at the RPE layer looked higher in the aged subject, which was confirmed by the en face maps at the RPE segment (b and f). The median [range], mean ± SD, and COV was 0.17 [0.000–0.49], 0.17 ± 0.048, and 0.28 in b, and 0.36 [0.000–0.67], 0.36 ± 0.07, and 0.19 in f, respectively. The en face map at the superficial choroid (c and g) or the total choroid (d and h) did not show such a remarkable difference. The pseudo-color map of the entropy covered full range from 0 to 1 in which the entropy was defined. *Scale bar:* 500 µm. The *color scale* in the upper right represents entropy [AU].

the RPE increased with age especially in eyes without PSD in the fellow eyes (See Supplementary Fig. S5).

Discussion

In the present study, we investigated the three-dimensional distribution of melanin-related pigmentation in the RPE and the choroid, using PS-OCT. The distribution of polarimetric entropy changed with eccentricity, with higher polarimetric entropy in the center and lower polarimetric entropy in the outer ring in the RPE layer, but the finding was not observed at the choroidal layer. The polarimetric entropy in the RPE was significantly associated with age in each area, while that in the choroid was not. The polarimetric entropy was negatively associated with axial

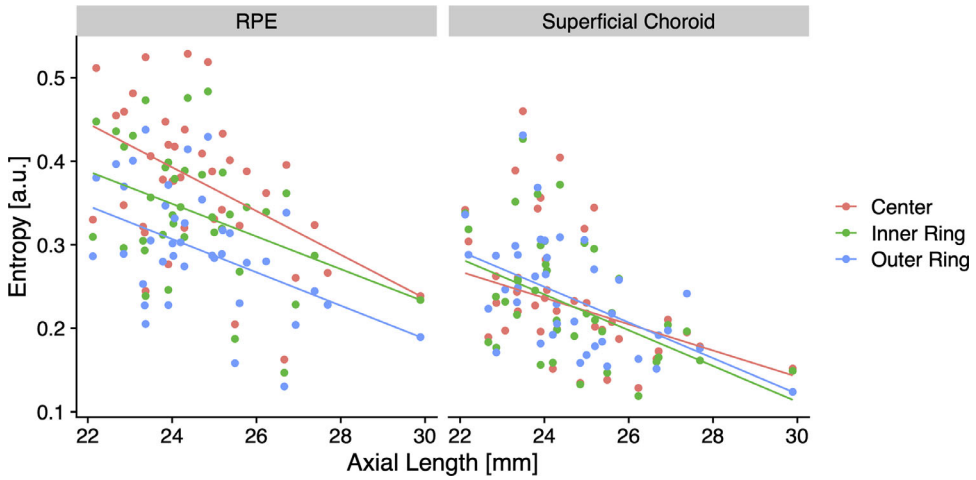

Figure 5. Scatter plots showing the relationship between axial length and the entropy in the center (*red*), the inner ring (*green*), or the outer ring (*blue*) at the RPE (*left*) and the superficial choroid layer (*right*). *Red line*, *green line*, or *blue line* were the regression lines from the data in the center, the inner ring, or the outer ring, respectively. Axial length showed fair correlation with the entropy in the RPE in all areas, center, inner ring, outer ring ($r = -0.37$ [$P = 0.02$], $r = -0.38$ [$P = 0.02$], $r = -0.41$ [$P = 0.01$], respectively; Spearman's rank correlation coefficient). Axial length also showed fair correlation with the entropy in the superficial choroid layer in all areas ($r = -0.54$ [$P = 0.004$], $r = -0.48$ [$P = 0.002$], $r = -0.56$ [$P < 0.001$], respectively; Spearman's rank correlation coefficient).

length in each area of the RPE and the superficial choroid. Sex or having PSD in the fellow eye was not associated with the polarimetric entropy. PS-OCT can examine the relationship between melanin distribution and lesions in three dimensions. Furthermore, quantitative analysis of polarimetric entropy may allow for more sensitive detection of retinal disease onset and progression. In view of validating the clinical usefulness of the device in the current study, defining the normal limits of each parameter so that the study eye could be compared to detect abnormality is also highly helpful. However, as a prerequisite for quantitative analysis of changes in melanin distribution in diseased eyes, it should be necessary to distinguish changes because of background factors such as age and gender that are within the physiological range. Although previous studies suggested that several background factors might alter melanin distribution, it is not clarified in detail. Furthermore, the distribution of melanin in the choroid is unknown. Therefore this study was conducted to examine the melanin distribution in the RPE and the choroid in normal eyes using depth-resolved PS-OCT and to obtain fundamental data and knowledge for quantitative analysis of melanin distribution. Using PS-OCT, only Baumann et al.[36] and Cense et al.[39] assessed melanin with clear separation of RPE. However, Bauman only looked at the RPE in 10 cases of 20 eyes, and Cense suggested a difference by age group, but it was inconclusive. We thus analyzed whether they needed to be corrected for age, axis length, and gender. To the best of our knowledge, there have been no reports on the analysis of the choroid as well as the RPE using PS-OCT as in the present study. Additionally, because it was initially confirmed that the distribution of melanin in the RPE differed centripetally, the following studies were conducted for each of the region, center, inner ring, and outer ring.

Spatial Distribution of Melanin Pigmentation

Polarimetric entropy in the RPE layer showed a decrease from the center to the periphery. Baumann et al.[36] analyzed the depolarization of normal human volunteer eyes using spectral domain PS-OCT. They used the DOPU to determine the degree of depolarization and reported that the minimum DOPU was most pronounced in the area close to the fovea. DOPU increased with eccentricity. Our results were consistent with those previously reported. These findings were attributed to the larger number of melanin granules in each RPE cell or denser packing of RPE cells at the macula.

On the other hand, the distribution of depolarization in the superficial or the total choroid layers was different from that observed in the RPE. The RPE, similar to ganglion substantia nigra, is derived from the neuroepithelium; however, the choroid (similar to the skin) is derived from the neural crest.[4] Such different embryological origins may lead to different distributional characteristics between the RPE and the choroid. Histologic analysis showed that choroid

melanin gradually increased from the equator to the posterior pole, with the highest concentration recorded in the macular area.[4] However, the detailed distribution at the macula was unclear. In the present analysis using PS-OCT, the mean polarimetric entropy in the superficial choroid layer was similar between the center, inner, and outer rings (within 6 mm in diameter). Meanwhile, the average polarimetric entropy in the total choroid layer was higher in the outer ring than the other two areas. A previous pathological analysis reported that the melanin pigment was distinctly distributed in the inner and outer choroid, with the latter containing approximately threefold higher levels of melanin than the former.[4] The current results from PS-OCT may reflect the difference in the distribution of melanin between the inner and outer choroid.

Association With Age

In the present study, melanin-related depolarization (measured using PS-OCT) increased with age. Previously, Cense et al.[39] suggested a difference by age group, but it was inconclusive. Melanin granules are classified into the pure type (melanosome) and complex (melanolipofuscin).[13,58] The melanosome decreases with age, while the complex type shows varying formation and increases with age.[13,58] Age-related change in the total amount of melanin after birth was unclear.[59,60] However, it was suggested that melanogenesis might occur throughout life in human RPE.[59] Although pure melanin granules are transformed to melanolipofuscin or melanolysosomes with age, melanin synthesis can occur in complex granules.[13,60,61] Therefore the current results, showing that depolarization in the RPE layer increased with age, may reflect increased melanolipofuscin granules in the RPE. A previous study reported that melanolipofuscin density was highest in the extrafovea and decreased toward the center or the periphery.[13] This may partly explain the present study results indicating that the relative polarimetric entropy of the outer ring to the center increased with age. In turn, the polarimetric entropy in the superficial choroid or the total choroid did not change with age in the present study. These findings were consistent with those obtained from a previous study using NIRAF,[16] but NIRAF image could not separate melanin from the RPE and the choroid clearly.

Association With Axial Length or Other Variables

In the RPE and the superficial choroid layers, the polarimetric entropy was negatively associated with axial length in all three areas, which has not been mentioned in the previous studies using PS-OCT to the best of our knowledge. In general, the eyes with longer axial length tended to have fewer cells within the area defined in the metric unit (1.5, 3, or 6 mm) than those with shorter axial length.[62] Such a "stretch effect" could cause the negative association between the polarimetric entropy in the RPE or the choroid and axial length, as shown in the present study.

We investigated the association with the presence of PSDs in the fellow eye. PSD includes CSC, pachychoroid pigment epitheliopathy, pachychoroid neovasculopathy, or FCE, which share some anatomical features (e.g., diffuse or focal thickening of the choroid, choroidal vessels, or RPE abnormalities).[54] Although multimodal imaging in the current study showed no abnormality in the eyes, several studies reported that the fellow eye of the subjects with unilaterally affected PSD tended to have a choroidal vascular abnormality.[63–65] In the present study, we tested the hypothesis that PSD in the fellow eye may be associated with distinct melanin distribution. Consequently, PSD in the fellow eye was not associated with the polarimetric entropy in the RPE, the superficial choroid, or the total choroid. Nevertheless, more detailed analysis is necessary to understand melanin's contribution to the pathophysiology of diseases such as PSD.

There were several limitations in the current study. First, the number of eyes included in this study was limited. Second, we need to investigate the mechanisms through which a variety of macular diseases influence the polarimetric entropy in the future. Third, the unaffected eyes of the subjects might have been potentially abnormal because the unstudied fellow eyes were diseased. Fourth, our method did not measure the thickness of the RPE. Because the thickness of the RPE or the choroid of interest could have variable thickness, ideally, the thickness of the tissue should be first measured and the melanin concentration should be assessed based on the thickness. However, in the present study, the RPE layer was identified using the maximum intensity of the A-scan and the localization of the inner or outer border of the RPE layer was not available. We thus assessed melanin pigmentation of the RPE layer using fixed thickness value. Additionally, it would be better to segment the choriocapirallis or the Sattler layer for melanin quantification, but it was not available in the current settings of our study. We are aiming at the melanin quantification using variable thickness of the RPE or the sublayer in the choroid for future analysis. Although the current study was performed in Asians, the influence of dark and light eyes on the melanin distribution should be of great interest and be clarified in future

studies. Moreover, it should be essential to investigate whether PS-OCT device could pick up more subtle changes caused by various pathological processes than conventional clinical settings. This issue was addressed partly by the previous studies[27,28,33–35] and is also of great importance for our following investigations. In the current study, we focused on the influences of various background factors such as age or axial length to investigate how much the entropy or melanin distribution could vary physiologically. The result of the current analysis was helpful as the fundamental data for studying diseases or subclinical pathologic conditions and strengthening the ability to detect subtle "pathological" changes. It should be necessary to investigate the usefulness in clinical settings based on these findings.

In conclusion, we were able to evaluate the polarimetric entropy through PS-OCT, reflecting the volumetric distribution of melanin concentration. The analysis revealed a difference in the distribution of melanin pigmentation between the RPE and the choroid. Polarimetric entropy measured using PS-OCT has potential utility to diagnose and predict the prognoses of retinochoroidal diseases related to melanin pigmentation distribution.

Acknowledgments

Supported by AMED under Grant Number JP19he1302011.

Disclosure: **A. Fujita,** None; **T. Amari,** None; **K. Ueda,** None; **K. Azuma,** None; **T. Inoue,** None; **K. Komatsu,** None; **M. Yamamoto,** None; **N. Aoki,** Tomey (E, P); **M. Yamanari,** Tomey (E, P); **S. Sugiyama,** Tomey (E, P); **M. Aihara,** None; **S. Kato,** None; **R. Obata,** None

References

1. Kollias N, Sayre RM, Zeise L, Chedekel MR. New trends in photobiology: Photoprotection by melanin. *J Photochem Photobiol B*. 1991;9:135–160.
2. Sarna T. New trends in photobiology: Properties and function of the ocular melanin — a photobiophysical view. *J Photochem Photobiol B*. 1992;12:215–258.
3. Ansorge M, Sahlmann B, Stanka P. On the melanization of the rat's eye. *Pigment Cell Res*. 1996;9:142–147.
4. Weiter JJ, Delori FC, Wing GL, Fitch KA. Retinal pigment epithelial lipofuscin and melanin and choroidal melanin in human eyes. *Invest Ophthalmol Vis Sci*. 1986;27:145–152.
5. Huang ZC, Zeng H, Hamzavi I, et al. Cutaneous melanin exhibiting fluorescence emission under near-infrared light excitation. *J Biomed Opt*. 2006;11:34010.
6. Mansour AM, Chhablani J, Arevalo JF, et al. Retinal detachment in albinism. *Clin Ophthalmol*. 2018;12:651–656.
7. Ostrovsky MA, Sakina NL, Dontsov AE. An antioxidative role of ocular screening pigments. *Vis Res*. 1987;27:893–899.
8. Kokkinou D, Kasper HU, Schwarz T, Bartz-Schmidt KU, Schraermeyer U. Zinc uptake and storage: the role of fundus pigmentation. *Graefes Arch Clin Exp Ophthalmol*. 2005;243:1050–1055.
9. Sarangarajan R, Apte SP. Melanization and phagocytosis: implications for age related macular degeneration. *Mol Vis*. 2005;11:482–490.
10. Rao NA. Pathology of Vogt-Koyanagi-Harada disease. *Int Ophthalmol*. 2007;27:81–85.
11. Du L, Kijlstra A, Yang P. Vogt-Koyanagi-Harada disease: Novel insights into pathophysiology, diagnosis and treatment. *Prog Retin Eye Res*. 2016;52:84–111.
12. Sarna T, Burke JM, Korytowski W, et al. Loss of melanin from human RPE with aging: possible role of melanin photooxidation. *Exp Eye Res*. 2003;76:89–98.
13. Feeney-Burns L, Hilderbrand ES, Eldridge S. Aging human RPE: morphometric analysis of macular, equatorial, and peripheral cells. *Invest Ophthalmol Vis Sci*. 1984;25:195–200.
14. Durairaj C, Chastain JE, Kompella UB. Intraocular distribution of melanin in human, monkey, rabbit, minipig and dog eyes. *Exp Eye Res*. 2012;98:23–27.
15. Schmidt SY, Peisch RD. Melanin concentration in normal human retinal pigment epithelium. Regional variation and age-related reduction. *Invest Ophthalmol Vis Sci*. 1986;27:1063–1067.
16. Keilhauer CN, Delori FC. Near-infrared autofluorescence imaging of the fundus: visualization of ocular melanin. *Invest Ophthalmol Vis Sci*. 2006;47:3556–3564.
17. Weinberger AW, Lappas A, Kirschkamp T, et al. Fundus near infrared fluorescence correlates with fundus near infrared reflectance. *Invest Ophthalmol Vis Sci*. 2006;47:3098–3108.
18. Paavo M, Zhao J, Kim HJ, et al. Mutations in GPR143/OA1 and ABCA4 Inform Interpretations of Short-Wavelength and Near-Infrared

Fundus Autofluorescence. *Invest Ophthalmol Vis Sci*. 2018;59:2459–2469.
19. Oguchi Y, Sekiryu T, Takasumi M, Hashimoto Y, Furuta M. Near-infrared and short-wave autofluorescence in ocular specimens. *Jpn J Ophthalmol*. 2018;62:605–613.
20. Cideciyan AV, Swider M, Jacobson SG. Autofluorescence imaging with near-infrared excitation: normalization by reflectance to reduce signal from choroidal fluorophores. *Invest Ophthalmol Vis Sci*. 2015;56:3393–3406.
21. Grieve K, Gofas-Salas E, Ferguson RD, et al. In vivo near-infrared autofluorescence imaging of retinal pigment epithelial cells with 757 nm excitation. *Biomed Opt Express*. 2018;9:5946–5961.
22. Vienola KV, Zhang M, Snyder VC, et al. Microstructure of the retinal pigment epithelium near-infrared autofluorescence in healthy young eyes and in patients with AMD. *Sci Rep*. 2020;10:9561.
23. Meleppat RK, Zhang P, Ju MJ, et al. Directional optical coherence tomography reveals melanin concentration-dependent scattering properties of retinal pigment epithelium. *J Biomed Opt*. 2019;24:1–10.
24. Miura M, Makita S, Sugiyama S, et al. Evaluation of intraretinal migration of retinal pigment epithelial cells in age-related macular degeneration using polarimetric imaging. *Sci Rep*. 2017;7:3150.
25. Burns SA, Elsner AE, Mellem-Kairala MB, Simmons RB. Improved contrast of subretinal structures using polarization analysis. *Invest Ophthalmol Vis Sci*. 2003;44:4061–4068.
26. VanNasdale DA, Elsner AE, Malinovsky VE, et al. Polarization Variability in Age-related Macular Degeneration. *Optom Vis Sci*. 2018;95:277–291.
27. Miura M, Yamanari M, Iwasaki T, et al. Imaging polarimetry in age-related macular degeneration. *Invest Ophthalmol Vis Sci*. 2008;49:2661–2667.
28. Miura M, Elsner AE, Weber A, et al. Imaging polarimetry in central serous chorioretinopathy. *Am J Ophthalmol*. 2005;140:1014–1019.
29. de Boer JF, Milner TE, van Gemert MJ, Nelson JS. Two-dimensional birefringence imaging in biological tissue by polarization-sensitive optical coherence tomography. *Opt Lett*. 1997;22:934–936.
30. Yamanari M, Tsuda S, Kokubun T, et al. Estimation of Jones matrix, birefringence and entropy using Cloude-Pottier decomposition in polarization-sensitive optical coherence tomography. *Biomed Opt Express*. 2016;7:3551–3573.
31. Pircher M, Gotzinger E, Findl O, et al. Human macula investigated in vivo with polarization-sensitive optical coherence tomography. *Invest Ophthalmol Vis Sci*. 2006;47:5487–5494.
32. Pircher M, Hitzenberger CK, Schmidt-Erfurth U. Polarization sensitive optical coherence tomography in the human eye. *Prog Retin Eye Res*. 2011;30:431–451.
33. Schutze C, Teleky K, Baumann B, et al. Polarisation-sensitive OCT is useful for evaluating retinal pigment epithelial lesions in patients with neovascular AMD. *Br J Ophthalmol*. 2016;100:371–377.
34. Schutze C, Wedl M, Baumann B, et al. Progression of retinal pigment epithelial atrophy in antiangiogenic therapy of neovascular age-related macular degeneration. *Am J Ophthalmol*. 2015;159:1100–1114.e1101.
35. Miura M, Makita S, Yasuno Y, et al. Polarization-sensitive optical coherence tomographic documentation of choroidal melanin loss in chronic Vogt-Koyanagi-Harada disease. *Invest Ophthalmol Vis Sci*. 2017;58:4467–4476.
36. Baumann B, Gotzinger E, Pircher M, Hitzenberger CK. Measurements of depolarization distribution in the healthy human macula by polarization sensitive OCT. *J Biophotonics*. 2009;2:426–434.
37. Baumann B, Baumann SO, Konegger T, et al. Polarization sensitive optical coherence tomography of melanin provides intrinsic contrast based on depolarization. *Biomed Opt Express*. 2012;3:1670–1683.
38. Baumann B, Schirmer J, Rauscher S, et al. Melanin pigmentation in rat eyes: in vivo imaging by polarization-sensitive optical coherence tomography and comparison to histology. *Invest Ophthalmol Vis Sci*. 2015;56:7462–7472.
39. Cense B, Miller DT, King BJ, Theelen T, Elsner AE. Measuring polarization changes in the human outer retina with polarization-sensitive optical coherence tomography. *J Biophotonics*. 2018;11:e201700134.
40. Hee MR, Huang D, Swanson EA, Fujimoto JG. Polarization-sensitive low-coherence reflectometer for birefringence characterization and ranging. *JOSA B*. 1992;9:903–908.
41. VanNasdale DA, Elsner AE, Hobbs T, Burns SA. Foveal phase retardation changes associated with normal aging. *Vis Res*. 2011;51:2263–2272.
42. Zhou Q, Leder H, Lo B, et al. Fundus depolarization imaging with GDx VCC scanning laser polarimeter and depolarization characteristics of normal eyes. *InOphthalmic Technologies XIX*. Bellingham, WA: International Society for Optics and Photonics; 2009:7163:71630L.

43. Papay JA, Elsner AE. Near-infrared polarimetric imaging and changes associated with normative aging. *J Opt Soc Am A Opt Image Sci Vis*. 2018;35:1487–1495.
44. de Boer JF, Hitzenberger CK, Yasuno Y. Polarization sensitive optical coherence tomography - a review [Invited]. *Biomed Opt Express*. 2017;8:1838–1873.
45. Lippok N, Braaf B, Villiger M, et al. Quantitative depolarization measurements for fiber-based polarization-sensitive optical frequency domain imaging of the retinal pigment epithelium. *J Biophotonics*. 2019;12:e201800156.
46. Lippok N, Villiger M, Bouma BE. Degree of polarization (uniformity) and depolarization index: unambiguous depolarization contrast for optical coherence tomography. *Opt Lett*. 2015;40:3954–3957.
47. Makita S, Kurokawa K, Hong YJ, Miura M, Yasuno Y. Noise-immune complex correlation for optical coherence angiography based on standard and Jones matrix optical coherence tomography. *Biomed Opt Express*. 2016;7:1525–1548.
48. Yamanari M, Mase M, Obata R, et al. Melanin concentration and depolarization metrics measurement by polarization-sensitive optical coherence tomography. *Sci Rep*. 2020;10:19513.
49. Yamanari M, Uematsu S, Ishihara K, Ikuno Y. Parallel detection of Jones-matrix elements in polarization-sensitive optical coherence tomography. *Biomed Opt Express*. 2019;10:2318–2336.
50. Yamanari M, Horikoshi K, Aoki N, et al. Optic axis determination in SU(2) Jones formalism. *InOptical Coherence Tomography and Coherence Domain Optical Methods in Biomedicine XXIII*. Bellingham, WA: International Society for Optics and Photonics; 2019;10867:108672F.
51. Bennett AG, Rudnicka AR, Edgar DF. Improvements on Littmann's method of determining the size of retinal features by fundus photography. *Graefes Arch Clin Exp Ophthalmol*. 1994;232:361–367.
52. Rasband WS. *ImageJ*. Bethesda, MD: U. S. National Institutes of Health. 1997–2018. Available at: https://imagej.nih.gov/ij/. Accessed December 10, 2020.
53. Blesh TE. *Measurement in Physical Education*. New York: The Ronald Press Company; 1974.
54. Cheung CMG, Lee WK, Koizumi H, et al. Pachychoroid disease. *Eye*. 2019;33:14.
55. Maruko I, Iida T, Sugano Y, Ojima A, Sekiryu T. Subfoveal choroidal thickness in fellow eyes of patients with central serous chorioretinopathy. *Retina*. 2011;31:1603–1608.
56. Ersoz MG, Karacorlu M, Arf S, Hocaoglu M, Sayman Muslubas I. Pachychoroid pigment epitheliopathy in fellow eyes of patients with unilateral central serous chorioretinopathy. *Br J Ophthalmol*. 2018;102:473–478.
57. Bartko JJ. The intraclass correlation coefficient as a measure of reliability. *Psychol Rep*. 1966;19:3–11.
58. Pollreisz A, Messinger JD, Sloan KR, et al. Visualizing melanosomes, lipofuscin, and melanolipofuscin in human retinal pigment epithelium using serial block face scanning electron microscopy. *Exp Eye Res*. 2018;166:131–139.
59. Boulton M, Docchio F, Dayhaw-Barker P, Ramponi R, Cubeddu R. Age-related changes in the morphology, absorption and fluorescence of melanosomes and lipofuscin granules of the retinal pigment epithelium. *Vision Res*. 1990;30:1291–1303.
60. Smith-Thomas L, Richardson P, Thody AJ, et al. Human ocular melanocytes and retinal pigment epithelial cells differ in their melanogenic properties in vivo and in vitro. *Curr Eye Res*. 1996;15:1079–1091.
61. Schraermeyer U. Does melanin turnover occur in the eyes of adult vertebrates? *Pigment Cell Res*. 1993;6:193–204.
62. Obata R, Yanagi Y. Quantitative analysis of cone photoreceptor distribution and its relationship with axial length, age, and early age-related macular degeneration. *PLoS One*. 2014;9:e91873.
63. Menchini U, Virgili G, Lanzetta P, Ferrari E. Indocyanine green angiography in central serous chorioretinopathy. ICG angiography in CSC. *Int Ophthalmol*. 1997;21:57–69.
64. Piccolino FC, Borgia L. Central serous chorioretinopathy and indocyanine green angiography. *Retina*. 1994;14:231–242.
65. Iida T, Kishi S, Hagimura N, Shimizu K. Persistent and bilateral choroidal vascular abnormalities in central serous chorioretinopathy. *Retina*. 1999;19:508–512.